

**EFFECT OF GRAIN REFINEMENT PROCESS USING EQUAL CHANNEL
ANGULAR PRESSING ON THE PROPERTIES AND CORROSION
BEHAVIOUR OF Sn-3.0Ag-0.5Cu SOLDER**

by

NUR ADRIANA NAZIFA BINTI ABU BAKAR

**Thesis submitted in fulfillment of the
requirement for the degree of
Master of Science**

JANUARY 2019

ACKNOWLEDGEMENTS

First and foremost, I would like to take this opportunity to express my gratitude to the Almighty God, Allah S.W.T for His blessing and strength for me to complete this master degree. I also would like to express my appreciation and sincere thanks to my supervisor and co-supervisor, Assoc. Prof. Dr. Nurulakmal bt Mohd Sharif and Dr. Tuti Katrina Abdullah, who have provided me the guidance and support throughout the pursuit of this master degree. Their valuable advice, constant guidance, willingness and encouragement are immeasurable.

My deepest appreciation goes out to the Dean of School of Materials and Mineral Resources Engineering, Prof. Zuhailawati Hussain. Thanks to the School of Materials and Mineral Resources Engineering for providing their equipment and other facilities which enables us to accomplish our project. And thanks to all the technicians who helped me throughout the experimental works.

I also would like to thank AUN-SEED/Net for the financial support. The funding has enable me to conduct the experimental work and finally complete the thesis. Last but not least, my gratitude also goes to those who indirectly contributed in this report writing, opinion and recommendations with the greatest wish, thank you very much.

Besides that, I would like to express my ultimate gratitude and respect to my family and friends for their encouragement and support throughout this work. Without you all, this thesis would not have been in its present form. THANK YOU.

TABLE OF CONTENTS

| | Page | |
|--|---|----|
| ACKNOWLEDGEMENTS | ii | |
| TABLE OF CONTENTS | iii | |
| LIST OF TABLES | vii | |
| LIST OF FIGURES | ix | |
| LIST OF ABBREVIATIONS | xiii | |
| LIST OF SYMBOLS | xvi | |
| ABSTRAK | xvii | |
| ABSTRACT | xix | |
| | | |
| CHAPTER ONE : INTRODUCTION | | |
| 1.1 | Research background | 1 |
| 1.2 | Problem statement | 2 |
| 1.3 | Objectives | 5 |
| 1.4 | Outline of thesis | 5 |
| | | |
| CHAPTER TWO : LITERATURE REVIEW | | |
| 2.1 | Soldering technology | 7 |
| 2.2 | Lead-free solder | 7 |
| | 2.2.1 Tin-silver-copper (Sn-Ag-Cu) solder alloy | 8 |
| 2.3 | Intermetallic compound (IMC) | 9 |
| 2.4 | Grain refinement | 9 |
| 2.5 | Severe plastic deformation (SPD) | 10 |
| 2.6 | Equal channel angular pressing | 10 |
| | 2.6.1 The shearing characteristics associated with ECAP | 13 |
| | 2.6.2 Influence of ECAP on IMCs (Zener pinning mechanism) | 17 |

| | | |
|-------|--|----|
| 2.6.3 | Influence of ECAP on crystallite size and lattice strain | 18 |
| 2.6.4 | Grain refinement and high angle grain boundaries by ECAP | 19 |
| 2.7 | Solderability | 23 |
| 2.7.1 | Spreading area/wetting angle | 23 |
| 2.8 | Mechanical testing | 24 |
| 2.8.1 | Microhardness test | 24 |
| 2.8.2 | Lap joint shear test | 26 |
| 2.9 | Corrosion behavior | 28 |
| 2.9.1 | Weight loss method | 29 |
| 2.9.2 | Potentiodynamic polarization | 30 |
| 2.9.3 | Type of corrosion products | 33 |
| 2.10 | Summary | 35 |

CHAPTER THREE : MATERIALS AND METHODOLOGY

| | | |
|-------|--|----|
| 3.1 | Introduction | 37 |
| 3.2 | Raw materials | 37 |
| 3.2.1 | SAC305 solder | 37 |
| 3.2.2 | Copper substrate | 39 |
| 3.2.3 | Flux | 39 |
| 3.3 | Sample preparation | 39 |
| 3.3.1 | Solder preparation | 39 |
| 3.3.2 | Substrate preparation | 41 |
| 3.3.3 | Reflow | 41 |
| 3.4 | Characterization of as-cast and ECAPed SAC305 solder | 42 |
| 3.4.1 | X-ray diffraction (XRD) | 42 |

| | | |
|-------|--|----|
| 3.4.2 | Scanning electron microscopy (SEM) | 43 |
| 3.4.3 | Electron backscatter diffraction (EBSD) | 44 |
| 3.4.4 | Spreading and wetting angle test | 46 |
| 3.4.5 | Microhardness test | 47 |
| 3.4.6 | Lap joint shear test | 48 |
| 3.4.7 | Immersion test | 49 |
| 3.4.8 | Potentiodynamic polarization | 51 |
| 3.4.9 | Surface examination study after corrosion test | 53 |

CHAPTER FOUR : RESULTS AND DISCUSSION

| | | |
|-------|--|----|
| 4.1 | Introduction | 54 |
| 4.2 | Preliminary characterization of as-cast SAC305 solder | 54 |
| 4.2.1 | Phase analysis | 54 |
| 4.2.2 | Microstructure of as-cast SAC305 solder | 55 |
| 4.3 | Selection of suitable number of ECAP process | 56 |
| 4.4 | Microstructural analysis of SAC305 solder at different ECAP Process | 58 |
| 4.5 | Electron backscatter diffraction (EBSD) measurements | 65 |
| 4.6 | X-ray diffraction analysis of SAC305 solder at different ECAP passes | 69 |
| 4.7 | Spreading and wetting angle test of SAC305 solder of different ECAP passes | 73 |
| 4.8 | Microhardness of SAC305 solder | 74 |
| 4.8.1 | Microhardness of bulk SAC305 solder | 74 |
| 4.8.2 | Microhardness of solder joint | 77 |
| 4.9 | Lap joint shear test of different ECAP passes | 79 |

| | | |
|--------|---|-----|
| 4.9.1 | Fractography of lap joint shear test | 81 |
| 4.10 | Immersion tests of different ECAP passes | 83 |
| 4.10.1 | Weight loss and surface observation of bulk solder | 83 |
| 4.10.2 | Weight loss and surface observation of solder joint | 93 |
| 4.11 | Potentiodynamic polarization at different ECAP passes | 102 |
| 4.11.1 | Potentiodynamic polarization of bulk SAC305 solder | 102 |
| 4.11.2 | Potentiodynamic polarization of SAC305 solder joint | 109 |
| 4.11.3 | Discussion of corrosion test results | 116 |

CHAPTER FIVE : CONCLUSION AND RECOMMENDATIONS

| | | |
|-----|-----------------|-----|
| 5.1 | Conclusion | 119 |
| 5.2 | Recommendations | 120 |

| | |
|-------------------|-----|
| REFERENCES | 122 |
|-------------------|-----|

APPENDIX

Appendix A : SEM Micrograph of Bulk Solder

Appendix B : SEM Micrograph of Intermetallic

Appendix C : Crystallite Size and Lattice Strain

Appendix D : Spreading Area and Wetting Angle

LIST OF PUBLICATION

LIST OF TABLES

| | | Page |
|------------|---|-------------|
| Table 2.1 | Definition of the rotations in the different processing routes for sixth pressing | 17 |
| Table 2.2 | Wetting categories of solder alloys | 24 |
| Table 2.3 | Constant value, K to evaluate corrosion rate of the materials | 29 |
| Table 2.4 | Constant value, K to evaluate metal loss of the materials | 29 |
| Table 3.1 | Chemical composition of SAC305 solder (wt.%) | 37 |
| Table 3.2 | Chemical compositions of the etching solution for bulk solder alloys | 43 |
| Table 3.3 | Example of weight percentage calculation | 44 |
| Table 3.4 | Weight percentage (wt.%) of possible IMC phases present | 44 |
| Table 4.1 | Example of weight percentage calculation | 63 |
| Table 4.2 | Weight percentage of possible phase present in SAC305 solder alloy | 63 |
| Table 4.3 | Full width at half maximum intensity (FWHM) of as-cast and ECAPed SAC305 solder | 71 |
| Table 4.4 | Spreading area and wetting angle result | 73 |
| Table 4.5 | Microhardness measurement of bulk as-cast and ECAPed SAC305 solder | 75 |
| Table 4.6 | Microhardness values after reflow of as-cast and ECAPed SAC305 solder | 77 |
| Table 4.7 | Shear strength of as-cast and ECAPed SAC305 solder | 79 |
| Table 4.8 | Weight loss of as-cast and ECAPed SAC305 bulk solder | 83 |
| Table 4.9 | Corrosion rate of as-cast and ECAPed SAC305 bulk solder | 84 |
| Table 4.10 | Weight loss of as-cast and ECAPed SAC305 solder joint | 93 |
| Table 4.11 | Corrosion rate of as-cast and ECAPed SAC305 solder joint | 95 |
| Table 4.12 | Potentiodynamic polarization measurement of as-cast and ECAPed SAC305 bulk solder | 105 |

| | | |
|------------|--|-----|
| Table 4.13 | Potentiodynamic polarization measurement of as-cast and ECAPed SAC305 solder joint | 112 |
| Table 4.14 | Standard electrode potentials of Sn, Ag and Cu | 118 |

LIST OF FIGURES

| | | Page |
|-------------|---|-------------|
| Figure 2.1 | Schematics of ECAP process and zones of work piece deformation through an ECAP die with two internal angles ϕ and ψ | 11 |
| Figure 2.2 | The regions of the deformed sample | 12 |
| Figure 2.3 | The four different processing routes for repetitive pressing | 13 |
| Figure 2.4 | The deformation of a cubic element through an ECAP die using route A (a) single pressing and (b) second pressing | 14 |
| Figure 2.5 | The deformation of a cubic element through an ECAP die using route B (a) single pressing and (b) second pressing | 15 |
| Figure 2.6 | The 3 rd , 4 th and 5 th passage through an ECAP die (a) route B _A and (b) route B _C | 15 |
| Figure 2.7 | The deformation of a cubic element through an ECAP die using route C (a) single pressing and (b) second pressing | 16 |
| Figure 2.8 | Scanning electron micrograph of ZrO ₂ (8Y)-7 vol% Al ₂ O ₃ annealed for 2h at 1500°C | 18 |
| Figure 2.9 | 3D misorientation map of low CN Fe-20%Cr alloy after ECAP (a) one pass, (b) two passes route A, (c) two passes route B _C , (d) two passes route C, (e) four passes route A, (f) four passes route B _C , (g) four passes route C | 20 |
| Figure 2.10 | OM image of as-cast A11080 | 21 |
| Figure 2.11 | Color-coded orientation maps of deformed A11080 via ECAP at different number of passes, (a) 2 passes, (b) 4 passes and (c) 10 passes | 21 |
| Figure 2.12 | Color-coded grain boundaries maps of deformed A11080 via ECAP, (a) 2 passes, (b) 4 passes and (c) 10 passes (high angle $\geq 15^\circ$ with blue line and low angle $< 15^\circ$ with red line) | 22 |
| Figure 2.13 | Schematic of the Vickers microhardness | 25 |
| Figure 2.14 | The average microhardness and standard deviation of as-cast and deformed A11080 up to 2, 4 and 10 passes | 26 |
| Figure 2.15 | Schematics of single lap joint | 27 |
| Figure 2.16 | Effect of number ECAP passes on ultimate tensile strength (UTS), 0.2% proof strength and elongation | 28 |

| | | |
|-------------|---|----|
| Figure 2.17 | The corrosion rate measurement of A11080 sample in 3.5 wt.% NaCl solution using mass loss method | 30 |
| Figure 2.18 | Potentiodynamic polarization curves SA, SAC105 and SAC305 solder alloys in 3.5 wt.% NaCl solution | 32 |
| Figure 2.19 | Microstructure of (a) as prepared SAC305 solder, after potentiodynamic polarization in (b) 1.0M HCl and (c) 3.5 wt.% NaCl | 34 |
| Figure 3.1 | Summary of experimental procedures | 38 |
| Figure 3.2 | Melting profile of SAC305 solder alloy | 40 |
| Figure 3.3 | A schematic of reflow process | 42 |
| Figure 3.4 | Schematic arrangement of sample orientation in the SEM | 45 |
| Figure 3.5 | A schematic of specimen for wetting angle and spreading test | 47 |
| Figure 3.6 | (a) INSTRON universal testing machine, (b) Lap joint shear test set up | 48 |
| Figure 3.7 | Dimension of specimen of lap joint shear test (in mm), (a) dimension of specimen and (b) side view of lap joint samples | 49 |
| Figure 3.8 | Schematic diagram of immersion test | 51 |
| Figure 3.9 | Potentiodynamic polarization of SAC305 solder, (a) actual and (b) schematic | 52 |
| Figure 4.1 | XRD pattern of bulk SAC305 solder | 55 |
| Figure 4.2 | Microstructure of as-cast of SAC305 solder alloy | 56 |
| Figure 4.3 | Microhardness of SAC305 solder at various number of ECAP passes at room temperature | 57 |
| Figure 4.4 | SEM micrograph of bulk as-cast SAC305 solder | 60 |
| Figure 4.5 | SEM micrograph of bulk 2 passes ECAPed SAC305 solder | 61 |
| Figure 4.6 | SEM micrograph of bulk 4 passes ECAPed SAC305 solder | 61 |
| Figure 4.7 | Microstructure of IMCs of SAC 305 solder alloy (a) as-cast, (b) 2 passes and (c) 4 passes | 64 |
| Figure 4.8 | Colour-coded orientation maps of SAC305 solder, (a) as-cast, and (b) deformed by ECAP up to 4 passes | 65 |

| | | |
|-------------|--|----|
| Figure 4.9 | Colour coded grain boundaries maps of SAC305 solder sample, (a) as-cast, and (b) deformed by ECAP up to 4 passes (high angle $\geq 15^\circ$ with yellow and blue lines and low angle $< 15^\circ$ with red and green lines) | 67 |
| Figure 4.10 | Misorientation angle distribution in SAC305 solder samples, (a) as-cast, and (b) processed by 4 passes of ECAP via B_C route | 68 |
| Figure 4.11 | XRD peak of as-cast and ECAPed SAC305 solder, (a) phase analysis and (b) peak broadening | 70 |
| Figure 4.12 | Crystallite size and lattice strain of as-cast and ECAPed SAC305 solder | 72 |
| Figure 4.13 | Microhardness measurement of as-cast and ECAPed SAC305 solder | 75 |
| Figure 4.14 | Schematic of microhardness measurement taken on solder joint | 77 |
| Figure 4.15 | Microhardness of as-cast and ECAPed SAC305 solder joint on Cu substrate | 78 |
| Figure 4.16 | Shear strength of as-cast and ECAPed SAC305 solder | 79 |
| Figure 4.17 | Morphologies of the fractography of as-cast and ECAPed SAC305 solder lap joint shear test, (a) as-cast, (b) 2 passes and (c) 4 passes | 82 |
| Figure 4.18 | Weight loss of as-cast and ECAPed SAC305 bulk solder | 84 |
| Figure 4.19 | Corrosion rate of bulk SAC305 for different ECAP passes | 85 |
| Figure 4.20 | Morphologies of the corrosion product of as-cast bulk solder, (a) 7 days, (b) 14 days, (c) 21 days and (d) 28 days | 88 |
| Figure 4.21 | Morphologies of the corrosion product of 2 passes ECAPed bulk solder, (a) 7 days, (b) 14 days, (c) 21 days and (d) 28 days | 89 |
| Figure 4.22 | Morphologies of the corrosion product of 4 passes ECAPed bulk solder, (a) 7 days, (b) 14 days, (c) 21 days and (d) 28 days | 90 |
| Figure 4.23 | XRD spectra of as-cast and ECAPed SAC305 bulk solder after immersion test, (a) as-cast, (b) 2 passes and (c) 4 passes | 91 |
| Figure 4.24 | Weight loss of as-cast and ECAPed SAC305 solder joint | 94 |
| Figure 4.25 | Corrosion rate of SAC305 solder joint for different ECAP passes | 95 |

| | | |
|-------------|---|-----|
| Figure 4.26 | Morphologies of the corrosion product of as-cast solder joint, (a) 7 days, (b) 14 days, (c) 21 days and (d) 28 days | 97 |
| Figure 4.27 | Morphologies of the corrosion product of 2 passes ECAPed solder joint, (a) 7 days, (b) 14 days, (c) 21 days and (d) 28 days | 98 |
| Figure 4.28 | Morphologies of the corrosion product of 4 passes ECAPed solder joint, (a) 7 days, (b) 14 days, (c) 21 days and (d) 28 days | 99 |
| Figure 4.29 | Phase analysis of as-cast and ECAPed SAC 305 solder joint after immersion test, (a) as-cast, (b) 2 passes and (c) 4 passes | 101 |
| Figure 4.30 | Potentiodynamic polarization curve of the as-cast SAC305 and deformed by ECAP in 3.5 wt.% NaCl solution for bulk solder | 104 |
| Figure 4.31 | Morphologies of bulk SAC305 solder after polarization (a,b) as-cast, (c,d) 2 passes and (e,f) 4 passes | 108 |
| Figure 4.32 | XRD spectra of SAC 305 bulk solder after polarization | 109 |
| Figure 4.33 | Potentiodynamic polarization curve curves of the as-cast SAC305 and deformed by ECAP in 3.5 wt.% NaCl solution for solder joint | 111 |
| Figure 4.34 | Morphologies of solder joint SAC305 after polarization (a,b) as-cast, (c,d) 2 passes and (e,f) 4 passes | 115 |
| Figure 4.35 | XRD spectra of SAC305 joint after polarization | 116 |

LIST OF ABBREVIATIONS

| | |
|--------------------------------|--|
| Ag | Silver |
| Al | Aluminium |
| Al ₂ O ₃ | Aluminium Oxide |
| ARB | Accumulative Roll Bonding |
| ASTM | American Society for Testing and Materials |
| Bi | Bismuth |
| CH ₄ O | Methanol |
| Cl | Chloride |
| Cr | Chromium |
| CR | Corrosion rate |
| Cu | Copper |
| CuCl | Copper Chloride |
| Cu ₂ O | Copper Oxide |
| DRX | Dynamic Recrystallization |
| EBSD | Electron Backscattered Diffraction |
| ECAE | Equal Channel Angular Extrusion |
| ECAP | Equal Channel Angular Pressing |
| EDX | Energy Dispersive X-ray |
| EPA | Environmental Protection Agency |
| Fe | Iron |
| FWHM | Full width at half maximum |
| g | gram |
| GPa | Giga pascal |
| HAGB | High angle grain boundaries |
| HCl | Hydrochloric acid |
| HNO ₃ | Nitric acid |
| HPT | High Pressure Torsion |
| hr | Hour |
| H ₂ O | Water |
| ICDD | International Centre for Diffraction Data |
| IMC | Intermetallic compound |

| | |
|--|---------------------------------------|
| in | Inch |
| In | Indium |
| LAGB | Low angle grain boundaries |
| mg | Milligram |
| ml | Millimetre |
| mm | millimeter |
| mmy | millimeter/year |
| MPa | Mega pascal |
| mpy | Mils/year |
| Na | Sodium |
| NaCl | Sodium chloride |
| NC/UFG | Nanocrystalline and ultrafine grained |
| nm | Nanometer |
| O | Oxygen |
| OM | Optical Microscope |
| Pb | Plumbum |
| PCB | Printed Circuit Board |
| Pt | Platinum |
| RA | Activated rosin flux |
| SAC305 | Sn-3.0Ag-0.5Cu |
| Sb | Antimony |
| SCE | Saturated calomel electrode |
| SEM | Scanning Electron Microscope |
| SHE | Saturated hydrogen electrode |
| Sn | Tin |
| SnCl ₂ | Tin Chloride |
| SnO | Tin Oxide |
| Sn ₃ O(OH) ₂ Cl ₂ | Tin Oxychloride |
| SPD | Severe Plastic Deformation |
| UFG | Ultrafine grain |
| UTS | Ultimate tensile strength |
| V | Vanadium |
| XRD | X-ray Diffraction |

| | |
|------------------|--------------------|
| XRF | X-ray Fluorescence |
| Zn | Zinc |
| ZnO ₂ | Zinc Oxide |

LIST OF SYMBOLS

| | |
|-------------------------------|--|
| $^{\circ}\text{C}$ | Degree celcius |
| $^{\circ}\text{C}/\text{sec}$ | Degree celcius per second |
| Wt.% | Weight percent |
| % | Percentage |
| ϕ | Channel intersection angle |
| Ψ | Arc of curvature angle |
| E | Strain |
| at.% | Atomic percent |
| λ | Wavelength |
| γ | Surface tension of solder |
| γ_{sl} | Surface tension between solid and liquid |
| γ_{lg} | Surface tension between liquid and gas |
| γ_{sg} | Surface tension between solid and gas |
| σ | Friction stress |
| τ | Crystallite size |
| μm | Micrometer |
| A | Area |
| Θ | Wetting angle |
| D | Grain size |
| E_{corr} | Corrosion potential |
| I_{corr} | Corrosion current |
| I_{pp} | Pseudopassivation current density |
| H | Hardness |
| K | Constant |
| kgf | Kilogram-force |
| N | Total number of pass |
| P | Standardized load |
| sec | Second |
| T_{m} | Melting temperature |

**KESAN PROSES PENGECILAN BUTIR MENGGUNAKAN PENEKANAN
SALURAN SEKATA BERSUDUT TERHADAP SIFAT DAN KELAKUAN
KAKISAN Sn-3.0Ag-0.5Cu PATERI**

ABSTRAK

Disebabkan oleh keracunan plumbum, undang-undang alam sekitar telah menguat kuasakan penghapusan penggunaan pateri berasaskan plumbum dalam peranti elektronik. Aloi Sn-Ag-Cu cenderung untuk dipilih kerana ia mempunyai sifat-sifat mekanikal dan kebolehbasahan yang baik serta takat lebur yang rendah. Walau bagaimanapun, kebolehharapan aloi SAC masih menjadi perhatian yang serius terutamanya apabila terdedah kepada haba atau dalam persekitaran yang menghakis pada jangka masa panjang. Penekan saluran sekata bersudut (PSSB) dapat digunakan sebagai proses untuk mengecilkan butir bagi meningkatkan rintangan kakisan dan kebolehharapan sambungan pateri. Kajian ini bertujuan untuk menilai mikrostruktur, sifat mekanikal dan kelakuan kakisan aloi SAC305 terhadap PSSB sehingga 4 laluan. Dalam kajian ini, sifat mekanikal aloi SAC305 sehingga 4 laluan menunjukkan nilai tertinggi kekerasan (17.5 HV) dan kekuatan rincih (70.5 MPa). PSSB digunakan untuk mengubah mikrostruktur aloi SAC305 dengan mengurangkan saiz butir Sn kepada butir yang halus (5.51 μm) dan mematahkan Sebatian Antara Logam (SAL) iaitu Ag_3Sn dan Cu_6Sn_5 kepada pecahan kecil dan diserakkan dalam matrik Sn. Ia juga menunjukkan saiz kristalit terkecil (0.28 μm) dan terikan kekisi tertinggi (4.36×10^{-1}). PSSB pada 4 laluan menghasilkan kebolehbasahan yang lebih baik berdasarkan kawasan penyebaran terbesar dan sudut basahan terkecil berbanding yang lain. Hasil daripada pengecilan butir dan pengedaran SAL yang lebih baik menyebabkan pateri mempunyai kekerasan yang lebih tinggi selepas PSSB. Rintangan kakisan juga ditingkatkan berdasarkan pengurangan berat dan kadar kakisan terendah serta nilai

potensi kakisan lebih positif. Morfologi permukaan sampel ujian rendaman menunjukkan partikel berbentuk bulat dan kemudian digantikan dengan filem seperti akar. Sampel PSSB 4 laluan polarisasi potentiodynamik menunjukkan permukaan yang diliputi secara sekata oleh partikel berbentuk seperti plat, manakala sampel-sampel yang lain mengalami kakisan terpilih yang mana terdapat lubang pada permukaan sampel. Fasa dan analisis unsur mendedahkan pembentukan beberapa produk kakisan seperti SnO_2 , SnCl_2 and $\text{Sn}_3\text{O}(\text{OH})_2\text{Cl}_2$ pada permukaan sampel. Penambahan bilangan laluan boleh menggalakkan penghalusan butir sampel SAC305 dengan peningkatan sifat mekanikal, kelakuan pembolehbasaan dan kakian rintangan.

**EFFECT OF GRAIN REFINEMENT PROCESS USING EQUAL CHANNEL
ANGULAR PRESSING ON THE PROPERTIES AND CORROSION
BEHAVIOUR OF Sn-3.0Ag-0.5Cu SOLDER**

ABSTRACT

Due to the inherent toxicity of Pb, environmental regulations have been enforced to eliminate the usage of Pb-based solders in electronic devices. Sn-Ag-Cu alloys is an attractive candidate due to good mechanical properties, good wettability and low melting temperature. However, the reliability of SAC solders is still a serious concern especially under long term exposure to heat or in corrosive environment. There is potential to improve the corrosion behavior and increase solder joint reliability by using Equal Channel Angular Pressing (ECAP) as a grain refinement process. The aim of this project was to evaluate the microstructure, mechanical properties and corrosion behavior of SAC305 alloy subjected to ECAP up to 4 passes. In this study, the mechanical properties showed that the 4 passes ECAPed SAC305 alloy exhibited the highest hardness value (17.5 HV) with improvement of shear strength (70.5 MPa). ECAP was used to alter the microstructure of SAC305 alloy by reducing the large Sn dendrites into fine and equiaxed grains (5.51 μm). ECAP also was observed to result in smaller IMC particles and better distribution of them in the Sn matrix. It also showed the smallest crystallite size (0.28 μm) and the highest lattice strain (4.36×10^{-1}). ECAP process resulted in improved wettability based on largest spreading area and smallest wetting angle compared to the others. As a result of grain refinement and more evenly distributed IMCs, solder had higher hardness after ECAP. The corrosion resistance was also improved based on lowest weight loss, lowest corrosion rate and more positive value of corrosion potential. The morphology on surface of immersion test samples showed rounded shape particles and then was

replaced with root-like film. ECAP 4 passes sample after potentiodynamic polarization was uniformly covered with plate-like shape corrosion product while the other samples suffered from selective corrosion with evidence of pits on the surface. Phase and elemental analyses revealed the formation of several corrosion product such as SnO_2 , SnCl_2 and $\text{Sn}_3\text{O}(\text{OH})_2\text{Cl}_2$ on the surface. The increase number of passes can induced grain refinement in SAC305 samples with better mechanical properties, wettability behavior and corrosion resistance.

CHAPTER ONE

INTRODUCTION

1.1 Research background

Soldering is used for metal interconnections in the electronic material, preferably with solder material having melting point below 425 °C. As a joining material, solder provides electrical, thermal and mechanical continuity in electronic assemblies. The solder is usually melted and solidified creating a metal joint in order to produce an electrical connection by using thermosonic bonding or alternatively reflow process. The integrity of a solder joint is dependent on the performance and quality of the solder (Abteew & Selvaduray, 2000).

As some electrical device or electronic board are exposed to corrosive environments during service, corrosion behavior of solder joint become one of the important considerations for solder behavior in electronic packaging. For example, wire bonding or solder joint will be exposed directly to corrosion media, such as air, moisture, air pollutants from industry and oceanic environments. The electronic devices have been reported to have serious problem when they are used in a harsh environment such as oceanic environment rather than in normal environment (Li, et al., 2008). The researchers also reported that corrosion resistance of the solder strongly depends on the solders' microstructural characteristics. The presence of three phases (fine Ag_3Sn and Cu_6Sn_5 IMCs and $\beta\text{-Sn}$) have been observed to promote an increase in the corrosion resistance for lead-free solders (Song & Lee, 2006). This is because higher area ratio of anode (fine Sn phase) to cathode (fine Ag_3Sn phase) will reduce the driving corrosion on Sn phase (Wang, et al., 2012)

The development of methods for grain refinement has attracted much attention over the years (Valiev, et al., 2000). Materials with refined grains have superior

mechanical properties that include extraordinarily high yield strength, high hardness, improved toughness and ductility with increasing strain rate. Severe plastic deformation (SPD) is one of the possible ways to induce grain refinement in metals. SPD is a technique of metalworking process that involve using a large plastic straining introduced into a bulk metal in order to induce grain refinement without any significant changes in the overall dimensions of the work piece (Sanusi, et al., 2012). There are several SPD methods which is equal channel angular pressing (ECAP), high pressure torsion (HPT), accumulative roll bonding (ARB), multi-directional forging and asymmetric rolling.

ECAP is one of the most effective SPD processing techniques because it offers the potential for high strain rate super plasticity by effective grain refinement from macro-grained structures to the level of the submicron or nano-scale through a special die. This ECAP process was used to refine macro-grained and alter the microstructure of Sn-Ag-Cu solder alloy by reducing size of the dendrites into fine and equiaxed grains. Besides that, this process will also break Ag_3Sn needles into smaller fragments and lead to enhancement of the corrosion resistance of solder alloys. The smaller size of Ag_3Sn encouraged formation of more compact surface film of corrosion products on the surface, preventing further corrosion and increase the corrosion resistance (Zhu, et al., 2009).

1.2 Problem Statement

Sn-3.0Ag-0.5Cu (SAC305) solder is one of the most preferable candidate among other lead-free solders due to their low melting temperature ($\sim 217^\circ\text{C}$), better solderability and good mechanical properties. But there are several issues with SAC305 solder that must be taken into consideration. As solder joint serves as mechanical and electrical connection, reliability of the joint is critical for the

performance of the device. Exposure to corrosive environment is one of the risks to reliability especially if the device or electrical component is used in aggressive environment such as high humidity or in coastal atmosphere.

Many researchers have investigated the corrosion behavior of SAC305 solder to increase reliability of the solder. For example, the corrosion behavior of SAC305 solder was investigated by using as-received (referred to commercial SAC305 solder), and the melts were cooled to room temperature in air and furnace which is (referred to as air-cooled (AC) and furnace cooled (FC) SAC305 solder) (Wang, et al., 2014). From this research, they found that better corrosion resistance was shown by commercial SAC305 solder than AC and FC SAC305 solder in 3.5 wt.% NaCl solution at 60°C/100 % relative humidity condition. The commercial SAC305 solder had a more adherent and compact surface film of corrosion products than AC and FC solders. This happened due to smaller size of Ag_3Sn IMCs in commercial SAC305 solder which encouraged good corrosion resistance compared to AC and FC SAC305 solder. The oxide film which consists of SnO_2 and SnO existed at the outer layer of corrosion product on the surface and the finer Ag_3Sn IMCs particles were easily protected by the oxide film (Wang, et al., 2014). This suggests that refinement of both Sn-matrix and IMC particles lead to improved corrosion resistance of solder.

One of the methods that could be used to refine solder microstructure and ultimately improve the corrosion behavior in SAC305 solder is Equal-Channel Angular Pressing (ECAP). ECAP is one of the modern techniques utilizing severe plastic deformation (SPD) to fabricate bulk ultrafine grained (UFG) and nanostructured materials that will enhance their physical and mechanical properties. This process will also alter the microstructure of SAC305 solder by reducing the large Sn dendrites into fine and equiaxed grains. The grain refinement that formed via ECAP

process provides improvement in mechanical properties. For Sn-Ag-Cu lead-free solder, it has been found that Ag_3Sn precipitates are also present within the Sn matrix. Gong, et al., (2010) reported that during ECAP process, Ag_3Sn could be broken into small fragments and more uniformly distributed within Sn matrix which could result in better corrosion resistance in 3.5 wt.% NaCl solution compared to SAC solder with large Ag_3Sn structure.

There are several researchers studied the grain refinement fabricated by ECAP process to enhance the corrosion behavior of pure aluminium, bronze and others. Sadawy and Ghanem, (2016) reported the effect of reducing grain size by ECAP on the corrosion behavior of bronze alloy in 3.5 wt.% NaCl solution. The researchers found that ECAPed bronze alloy exhibited higher corrosion resistance than the as-cast bronze alloy. The corrosion resistance of bronze alloy is higher with increased ECAP number of passes.

Moreover, another researcher Abd El Aal and Sadawy, (2015) also reported similar enhancement on the corrosion behavior of pure aluminium. In their research, pure aluminium samples were processed via ECAP up to 10 passes. The ECAP process reduced the grain size from 390 μm for as-cast down to 1.8, 0.4, and 0.3 μm after ECAP up to 2, 4, and 10 passes respectively. The microhardness and tensile strength were increased with the increase of ECAP number of passes. The improvement in corrosion resistance of pure aluminium in 3.5 wt.% NaCl solution can be observed as the ECAP number of passes increased. This is because of further deformation via ECAP contributes to decrease of the grain size. Thus, the high fraction of grain boundaries in the pure aluminium reduces the corrosion rates by accelerating the passivation process and reducing the intensity of galvanic couple between grain interior and grain boundary.

However, there was limited explanation on why ECAP process was able to improve the corrosion resistance of SAC305 solder. Therefore, the present work focused on the effect of ECAP as a grain refinement technique on the microstructure of solder and also on the corrosion behavior. The focus is to study the correlation between grain refinement, fragmentation of IMC particles, and the corrosion resistance.

1.3 Objectives

The objectives of this project can be simplified as:

- To determine suitable number of passes for enhancement of mechanical properties via hardness test
- To analyze the effect of grain refinement on wettability and shear strength of SAC305 solder alloy
- To evaluate the corrosion behaviour of SAC305 solder alloy before and after ECAP process, and with number of ECAP passes

1.4 Outline of thesis

In this project, ECAP process was carried out to induce grain refinement in SAC305 solder. The focus is to evaluate the resultant microstructure and the grain refinement effect on wettability, hardness, shear strength of solder joint, and corrosion behavior of solder in NaCl environment. In order to do this, various characterization methods were employed: wettability test via wetting angle and spreading area, hardness via Vickers microhardness and shear strength of solder joint by using INSTRON machine. The resultant microstructure is characterized by using SEM and EDX with electron backscatter diffraction (EBSD). The phase analysis and broadening peak of bulk solder was determined by XRD analysis.

In this research, the corrosion behavior of bulk solder and reflowed solder joint were measured via immersion test for 28 days and potentiodynamic polarization (AUTOLAB PGSTAT). For immersion test, the weight of all bulk and solder joint were measured before and after immersion using weight balance to calculate the weight loss in every immersion periods. The results of weight loss were used to calculate the corrosion rate of each sample. The microstructure corrosion product of both test for all specimens were observed via SEM and EDX. The phase analysis of the corroded specimens was determined by XRD analysis. The resultant potentiodynamic polarization curve and the phase analysis of corroded products are expected to show deeper understanding on the corrosion behavior of ECAPed solder alloy and how grain refinement is able to alter the corrosion resistance.

CHAPTER TWO

LITERATURE REVIEW

2.1 Soldering technology

Soldering is a well known process used to metallurgically bond or joint two metal components using filler metal that has a melting point below 425°C. Soldering is used in order to provide interconnection in wiring board, printed circuit board, and assembly process. In electronic materials area, solder plays an important role for providing electrical, thermal and mechanical continuity in electronic assemblies. The integrity of solder joint is dependent on the performance and quality of the solder and how soldering is made (Abtew & Selvaduray, 2000). There are two common techniques of soldering which is used in electronic packaging which are wave and reflow soldering.

2.2 Lead-free solder

Sn-Pb solder has been used for many years for metal interconnections that have many advantages in electronic circuits. The selection of Sn-Pb in electronic industry is because of low melting temperature, low cost, satisfactory mechanical properties, excellent wetting on Cu substrate and ease for handling. Nevertheless, there are legal and environmental factors for Pb to be removed from electronic packaging. Environmental Protection Agency (EPA) stated that Pb is one of the chemicals that have high level of toxicity that effecting human life and the environment. Some important considerations are needed to ensure the performance of solder material for packaging applications is at least comparable or better than the Sn-Pb solders for which they are replacing.

- The melting temperature should be low in order to avoid thermal damage in electronic circuit.

- The wettability between the solder and the base metal is good, i.e solder properly wet the surface of substrate and form good joint.
- Good in mechanical properties (For example, tensile strength, hardness, creep).
- The alternative solder should not be of much higher cost compared to Sn-Pb solders.

Lead-free solders can be either binary alloys (Sn-Ag, Sn-Cu, and Sn-Zn alloys), ternary alloys (Sn-Ag-Cu, Sn-Zn-Ag, Sn-Zn-In alloys) or quaternary alloys (Sn-Zn-Ag-Al, Sn-Ag-Bi-Cu, and Sn-In-Ag-Sb alloys) (Osorio, et al., 2011). There are several alloys that have been reported to meet the said requirements, and there are include Sn-Ag, Sn-Cu and Sn-Ag-Cu (Wu, et al., 2004).

2.2.1 Tin-silver-copper (Sn-Ag-Cu) solder alloy

Among the candidates to replace Sn-Pb solder, Sn-Ag-Cu (SAC) solder alloys are considered as the most promising. SAC alloy has good solderability, high ductility, long fatigue life and beneficial electrical and mechanical properties. SAC also has lower melting temperature and good wettability as compared to the binary alloy, Sn-Ag. The addition of Cu typically in the range between 0.3 to 0.7 wt.% into Sn-Ag resulted in low melting temperature, i.e about 217°C - 220°C depending on the composition of elements (Liang, et al., 2007). The intermetallic compound of Cu_6Sn_5 and Ag_3Sn are observed to be present in the Sn-Ag-Cu. In the electronic industry, Sn-3.0Ag-0.5Cu (SAC305) has been widely used commercially in electronic packaging interconnections (Wang, et al., 2012).

2.3 Intermetallic compound (IMC)

Intermetallic compound (IMC) is a compound form when two or more metals combined, and the formation is subjected to specific chemical formula. In Sn-Ag-Cu alloys, two types of IMC which is Cu_6Sn_5 and Ag_3Sn are commonly formed in bulk solder. The formation of IMCs in solder joint can cause serious problem during service for the printed wiring boards. The IMCs are severally brittle and they can lead to deterioration of the mechanical properties of the solder joint especially at high load or under cyclic loading (Kim, et al., 2003). Kim, et al., (2002) reported the formation of IMCs with different size in Sn-3.0Ag-0.5Cu, Sn-3.5Ag-0.7Cu and Sn-3.9Ag-0.6Cu alloys by using three cooling conditions after casting process. It is found that the large Ag_3Sn platelets exhibited higher influence in decreasing the tensile properties in the solder alloys. Hence, the formation of Ag_3Sn and Cu_6Sn_5 should be controlled in order to optimize the superior mechanical properties of the solder alloys used in electronic industry.

2.4 Grain refinement

In recent years, grain refinement techniques have been attracting interest as they are seen as an effective method to fabricate materials with superior strength. Grain size can be regarded as key microstructure factor affecting almost all aspects of the physical and mechanical behavior of polycrystalline metals (Estrin and Vinogradov, 2013). Generally, small grain size offer many benefits rather than coarser grain size because their provide increment in strength, enhance ductility and creep resistance (Kashyap, 2014).

Therefore, control of the grain size is a way to design materials with desired properties. It is well known that the strength of polycrystalline materials can be related to size following with Hall-Petch equation as shown in Equation 2.1.

$$\sigma_0 = \sigma_1 + \frac{K}{\sqrt{D}} \quad \text{Equation 2.1}$$

Where σ_0 is the friction stress and K is a constant of yielding. From the equation, it is clear that the strength increases with a reduction of grain size.

2.5 Severe plastic deformation (SPD)

Severe plastic deformation has been attracting significant research interest over the last few years because it is an effective method to produce grain refinement in fully dense, bulk scale work pieces, thus giving promise for desired applications (Estrin and Vinogradov, 2013). SPD process is defined as any method of metal forming under an extensive hydrostatic pressure that may be used to impose a very high strain on a bulk solid without the introduction of any significant change in the overall dimensions of the sample and having the ability to produce exceptional grain refinement (Valiev, et al., 2006). Traditional methods of plastic deformation such as rolling, drawing or extrusion cannot meet certain requirements. These requirements include obtaining ultrafine grained structures with high angle grain boundaries. The materials also should not have any mechanical damage or cracks when subjected to large amount of deformation (Estrin and Vinogradov, 2013). Several methods are available such as equal-channel angular pressing (ECAP), accumulative roll-bonding (ARB) and high-pressure torsion (HPT). But the most attractive methods are ECAP and HPT. Both methods were able to introduce a high density of dislocations into the samples and the dislocations were rearranged to form an ultrafine grained submicrometer microstructure or a nanocrystalline structure (Figueiredo & Langdon, 2009).

2.6 Equal channel angular pressing (ECAP)

One of the method in controlling the size of grain and IMCs is by using grain refinement technique such as equal-channel angular pressing (ECAP) process. Equal

channel angular pressing (ECAP) or also known as equal channel angular extrusion (ECAE) is one of the SPD techniques to develop ultrafine grained and nanocrystalline structure in the materials. ECAP process was invented by Segal, et al., (1981) and has been proven as a successful method for fabricating fine grained bulk metals. The initial size and the shape of the materials are maintained and this is the advantage of this method (Watazu, 2011). A well lubricated billet is needed to minimize the friction during pressing. During the process, a simple shear strain is introduced to the sample when the billet pass through the plane where the two channels meet. This process is illustrated in Figure 2.1 which shows the ECAP process and zones of work piece deformation consists of two channels that are equal in cross section with an intersecting angle near the center of the die. Before the pressing, the sample is machined to fit within the channel and pressed by using a plunger (Furukawa, et al., 2001).

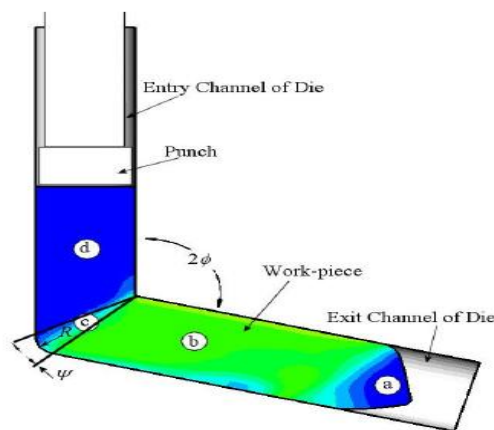


Figure 2.1: Schematics of ECAP process and zones of work piece deformation through an ECAP die with two internal angles ϕ and ψ (Patil, et al., 2008)

The precise values of the von Mises equivalent strain depends on the angle of the two channels when the sample passes through the ECAP die. The samples were

pressed repeatedly in order to achieve a very high total strain. The accumulating total strain in the samples can be calculated by using Equation 2.2.

$$\epsilon_N = N/\sqrt{3} [2 \cot (\phi/2 + \psi/2) + \phi \operatorname{cosec} (\phi/2 + \psi/2)] \quad \text{Equation 2.2}$$

where N is the total number of ECAP passes through the die. The deformed samples can be divided into three main regions which is shown in Figure 2.2 (Agwa, et al., 2016).

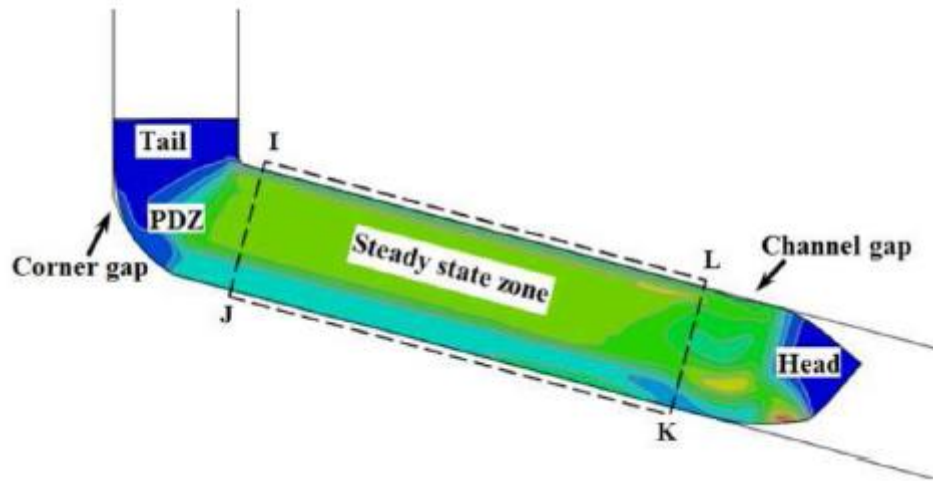


Figure 2.2: The regions of the deformed sample (Agwa, et al., 2016)

The regions in the deformed samples are important in order to optimize the processing parameters in ECAP process. From Figure 2.2, head is the front of the deformed sample, tail is the region at the back of the sample and steady state zone means the region where the strain is uniform along the deformed sample and billet axis (Agwa, et al., 2016). The repeated pressing of the samples without any significant change in the cross-section is one of the advantages in ECAP process. The modification of the shear plane and direction occurred due to the changing of the sample orientation after each pass. Hence the microstructure and texture of each

material can be controlled, thus altering the mechanical properties (Werenskiold, 2004).

2.6.1 The shearing characteristics associated with ECAP

The sample is pressed through the ECAP die and can be repeated depending on the materials and the required modification of properties. The shearing characteristic which is shearing plane and direction within the crystalline sample was changed by the rotation of sample for each pressing. There are several rotation modes in ECAP process, (i) no rotation, (ii) rotation by $+90^\circ$ or $\pm 90^\circ$ or (iii) rotation by $+180^\circ$ between pressing process. The various routes in ECAP process were shown in Figure 2.3 (Furukawa, et al., 2001).

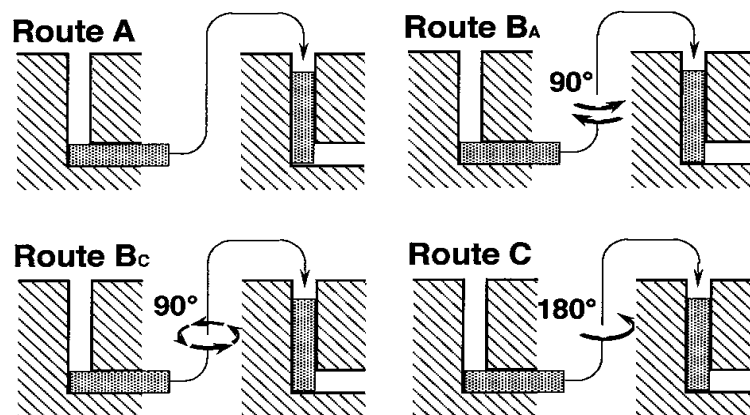


Figure 2.3: The four different processing routes for repetitive pressings (Furukawa, et al., 2001)

Based on Figure 2.3, route A shows that no rotation between repetitive pressings. Route B is carried out either by rotating the sample by 90° in alternate direction between each pressing known as B_A. On the other hand, the route B_C means that rotating of 90° in the same direction between each pressing of the sample. For route C is rotating of the sample by 180° between each individual pressing in ECAP. The deformation of the sample after passing through an ECAP die is illustrated in

Figures 2.4 to 2.7 in order to understand the shearing associated with these different processing routes using ECAP die with internal angles of $\phi = 90^\circ$ and $\psi = 0^\circ$ for route A (Furukawa, et al., 2001).

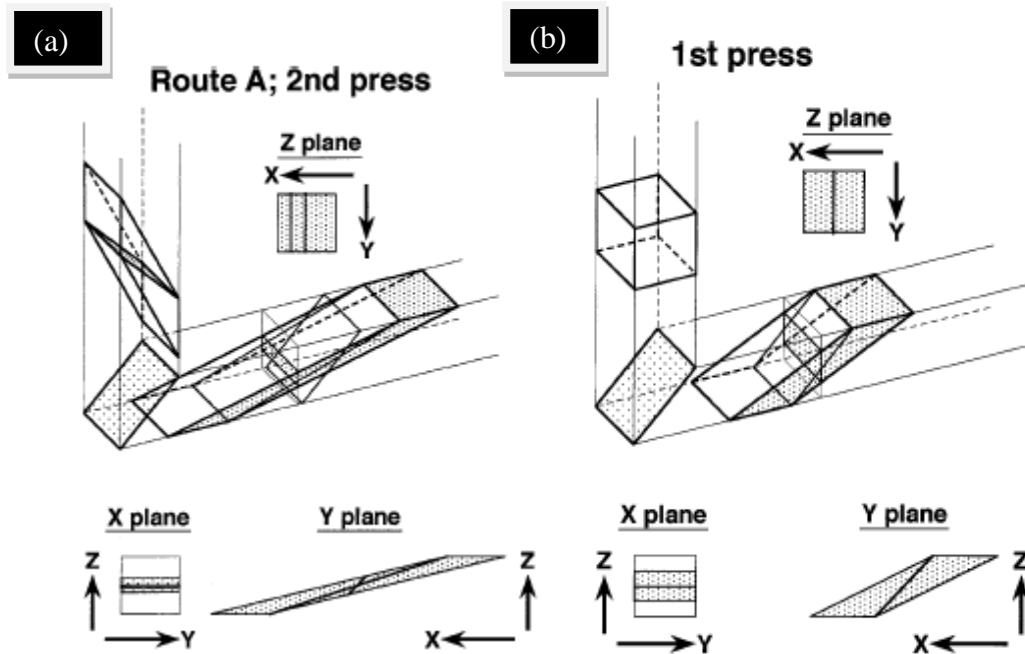


Figure 2.4: The deformation of a cubic element through an ECAP die using route A (a) single pressing and (b) second pressing (Furukawa, et al., 2001)

The first pressing produce grain elongation and the second pressing through route A with no rotation for each pressing markedly increased distortion of the rhombohedral shape. Route A was leading to the elongation of the grains in the y plane at an angle of $\sim 15^\circ$ to the x axis. As shown in Figure 2.5, route B is carried out by rotating at 90° that increases the distortion in the X and Z planes. Route B leads to elongations of grains in the materials on each orthogonal plane. For pressing using routes B_A and B_C for the 3rd, 4th and 5th passes are illustrated in Figure 2.6(a) and (b) respectively. The shearing characteristics of routes A and B_A are similar and lead to increases distortions of the original cubic elements. However, routes B_C and C are similar shearing characteristics with restoration of the cubic element (Furukawa, et al., 2001).

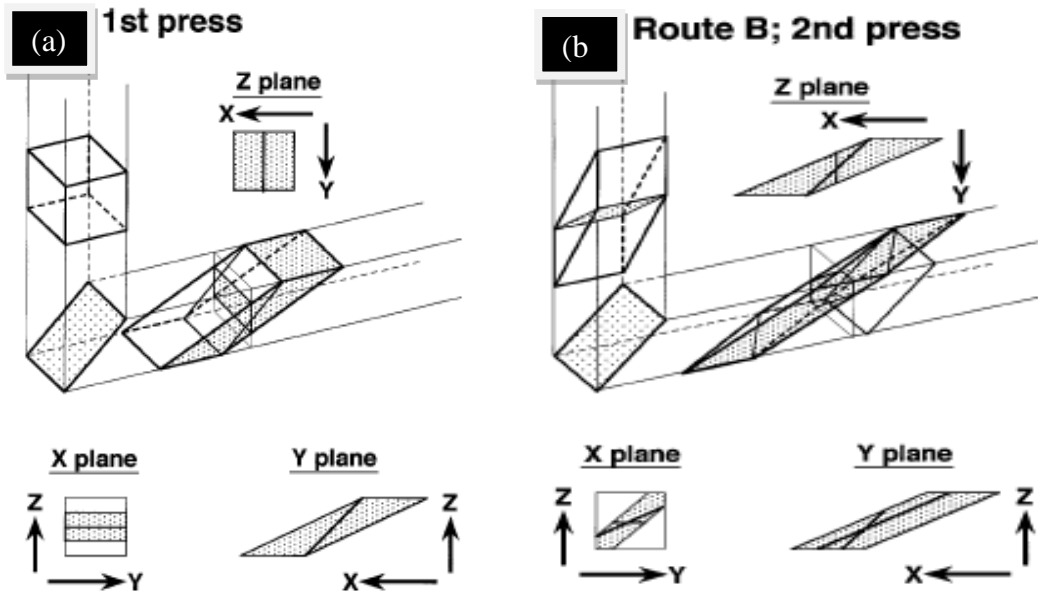


Figure 2.5: The deformation of a cubic element through an ECAP die using route B

(a) single pressing and (b) second pressing (Furukawa, et al., 2001)

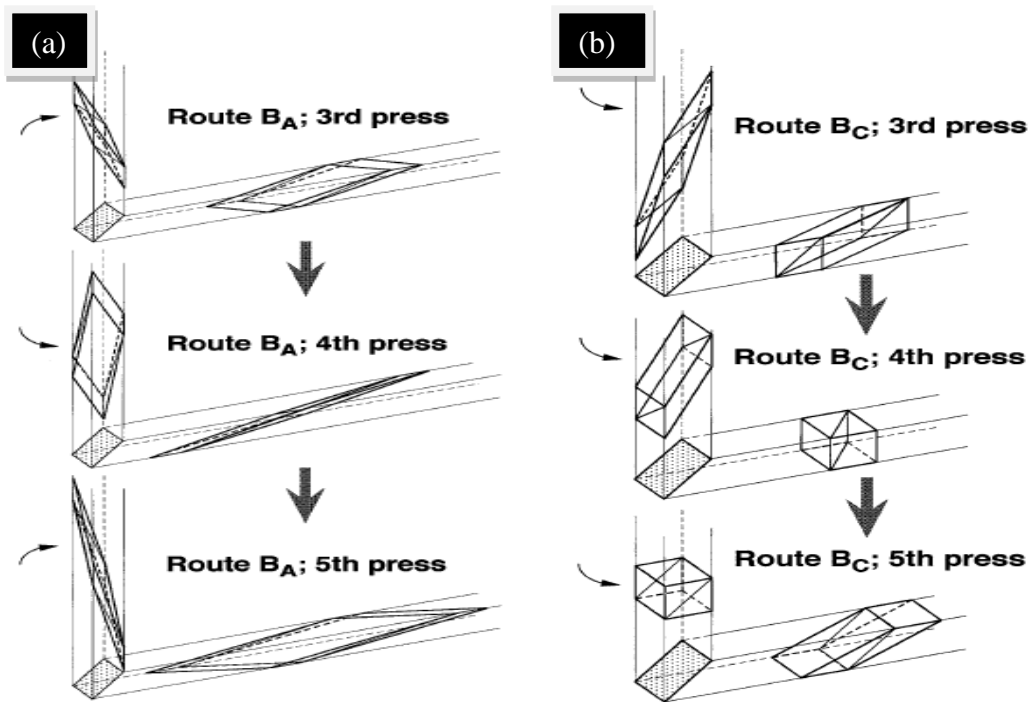


Figure 2.6: The 3rd, 4th and 5th passage through an ECAP die (a) route B_A and (b) route B_C (Furukawa, et al., 2001)

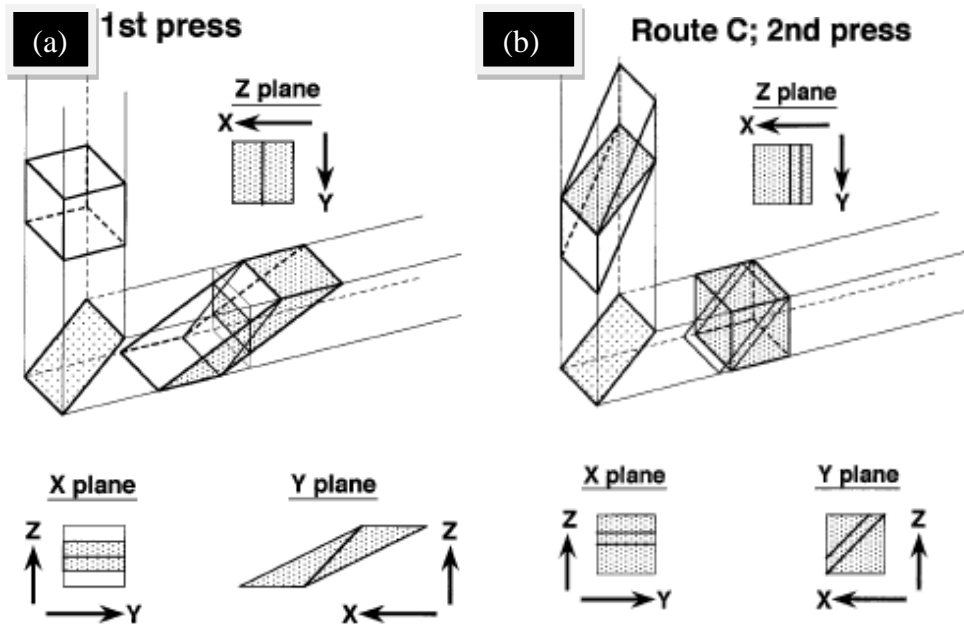


Figure 2.7: The deformation of a cubic element through an ECAP die using route C
 (a) single pressing and (b) second pressing (Furukawa, et al., 2001)

The cubic shape of the plane is being restored in deformation by using route C without any distortion of the bulk sample. There is no deformation occurred in the Z plane when using route C as shown in Figure 2.7. In order to make it more clear about the effect of rotation to the sample for sixth different processing routes can be determined in Table 2.1. The shearing characteristics in route B_A (0° - 90° - 0° - 90°) is similar to route A, while route B_C (0° - 90° - 180° - 270°) is similar to the route C. Then, route A had continuously changing in the x and y planes but no deformation in the Z plane of the cubic element. While, route B_A is changes in all three planes. On the other hand, the cubic element is restored after $4n$ passes in route B_C but $2n$ passes and no deformation in the z plane for route C, where n is an integer. The most preferable route is B_C and C due to the ultimate restoration of the cubic element rather than route B_A and A. Due to the lacking of deformation in the Z plane in route C making route B_C the most preferred route for ECAP process (Werenskiold, 2004).

Table 2.1: Definition of the rotations in six different processing routes (Werenskiold, 2004)

| Route | Number of pressings | | | | | | |
|-------------------|---------------------|-------|-------|-------|-------|-------|-------|
| | 2 | 3 | 4 | 5 | 6 | 7 | 8 |
| A | 0° | 0° | 0° | 0° | 0° | 0° | 0° |
| E _A | 90° ↶ | 90° ↷ | 90° ↶ | 90° ↷ | 90° ↶ | 90° ↷ | 90° ↶ |
| E _C | 90° ↶ | 90° ↶ | 90° ↶ | 90° ↶ | 90° ↶ | 90° ↶ | 90° ↶ |
| C | 180° | 180° | 180° | 180° | 180° | 180° | 180° |
| B _A -A | 90° ↶ | 0° | 90° ↷ | 0° | 90° ↶ | 0° | 90° ↷ |
| B _C -A | 90° ↶ | 0° | 90° ↶ | 0° | 90° ↶ | 0° | 90° ↶ |

2.6.2 Influence of ECAP on IMCs (Zener pinning mechanism)

The ECAP process is used in order to induce grain refinement in the microstructure. Typically, after ECAP, the microstructure showed breakage of the IMCs into smaller fragments that is more effective in pinning slip or dislocation motion. This is more commonly known as Zener pinning mechanism. The breakage of IMC particles, which in case of Sn-based solder are Ag₃Sn and Cu₆Sn₅ can impart improvement of mechanical properties. Zener pinning is the influence of dispersed fine particles on the movement of low and high angle grain boundaries through a polycrystalline material. The recovery, recrystallization and grain growth processes can also be influenced by Zener pinning. Small particles act to prevent the motion of such boundaries by exerting a pinning pressure which counteracts the driving force that pushes the boundaries (Zhou et al., 2017).

As an example, ZrO₂ particles has been used as additive to control grain growth behaviour during high-temperature annealing in alumina (Al₂O₃). The improvement in mechanical properties is caused by grain size refinement due to addition of zirconia. The growth of alumina grains is retarded by zirconia dispersion in alumina-rich matrix.

The zirconia particles which are mostly located at grain boundaries of Al_2O_3 matrix (shown in Figure 2.8) is regarded as the Zener's pinning effect. Therefore, the grain growth and grain refinement is dependent on distribution and size of zirconia particles within the materials (Okada and Sakuma, 1992).

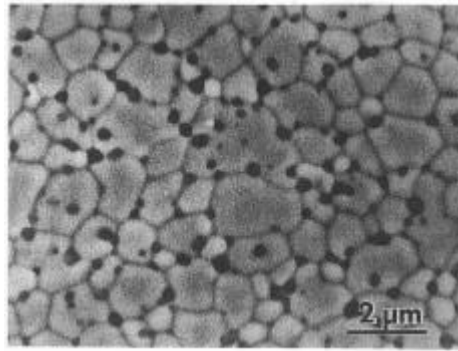


Figure 2.8: Scanning electron micrograph of $\text{ZrO}_2(8\text{Y})$ -7 vol% Al_2O_3 annealed for 2h at 1500°C (Okada and Sakuma, 1992)

2.6.3 Influence of ECAP on crystallite size and lattice strain

Severe plastic deformation by ECAP has become the most promising techniques in order to form materials with UFG structure. Alteration of microstructure in ECAPed samples including the crystallite size and lattice strain (at the atomic level) lead to broadening of the diffraction pattern shown in X-ray diffraction (XRD) analysis. When the crystallite size become smaller than about a micrometer, the diffracted pattern showed broadening of the major peak. The peak broadening is due to alteration in the lattice structure of the metal which resulted from small crystallite size in the growth direction of the strains, stacking faults, dislocations and point defects (Ungar, 2004).

The calculation of crystallite size and lattice strain based on broadening peak of the XRD analysis of the sample is done following the Scherrer method. The width of a diffraction peak broadening can be estimated by calculating the angular width, B

in radians at intensity equal to half maximum intensity (FWHM) (Zak, et al., 2011). Gubicza, et al., (2005) have analyzed the crystallite size, lattice strain and dislocation density of ECAP copper up to 1, 2, 4 and 8 passes using route C. The result showed that ECAP had refined the average crystallite size with the increased of dislocation density and increment of lattice strain ECAP passes increased. The crystallite size is reduced to 76 ± 8 nm while the dislocation density is increased from 8×10^{14} to 28×10^{14} m^{-2} when the strain increased from 0.7 to 4 (Gubicza, et al., 2005).

2.6.4 Grain refinement and high angle grain boundaries by ECAP

There are several researchers who reported using ECAP process in order to fabricate grain refinement structure. For example, Rifai, et al., (2014) reported the microstructural evolution during ECAP of low CN Fe-20%Cr alloy by observing the three orthogonal planes. This alloy was pressed at 423K from one, two and four passes using several routes which is A, B_C and C. It was shown that after 2 passes using route A, the structure was dominated by low angle grain boundaries (LAGB) with little fraction of high angle grain boundaries (HAGB) (Figure 2.9(b)-(d)). The 4 passes sample showed an increased of the fraction HAGB which replaced some LAGB (Figure 2.9(e)-(g)). In route A, a little fraction of HAGB existed in Z plane due to HAGB extended nearly parallel to Z-plane after the sample was processed up to 4 passes. The same observation was reported for sample pressed following route C. HAGB is more equally in orthogonal plane in route B_C as compared with routes A and C as shown in Figure 2.9(f). Thus, it was producing more equiaxial and isotropic structure in route B_C (Rifai, et al., 2014).

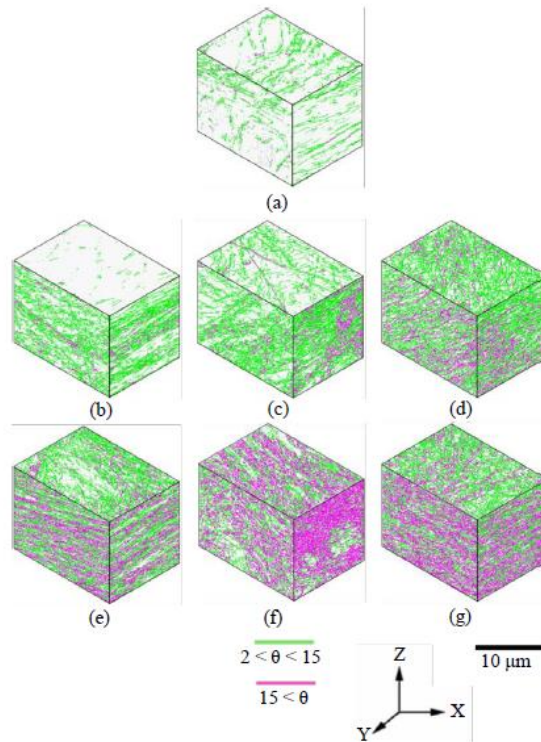


Figure 2.9: 3D misorientation map of low CN Fe-20%Cr alloy after ECAP (a) one pass, (b) two passes route A, (c) two passes route B_C, (d) two passes route C, (e) four passes route A, (f) four passes route B_C, (g) four passes route C (Rifai, et al., 2014)

The grain refinement effect via ECAP process was also reported by Abd El Aal and Sadawy, (2015) who investigated the microstructure on pure aluminium. The material was processed by ECAP up to 10 passes at room temperature in order to observe the microstructure evolution towards the number of ECAP passes. The observation of microstructure is carried out before and after ECAP process. The as-cast A11080 sample is shown in Figure 2.10 with an average grain size about 390 μm. An ECAP process is carried out using route A and the color-coded orientation maps of the deformed A11080 up to 2, 4 and 10 passes are shown in Figure 2.11.

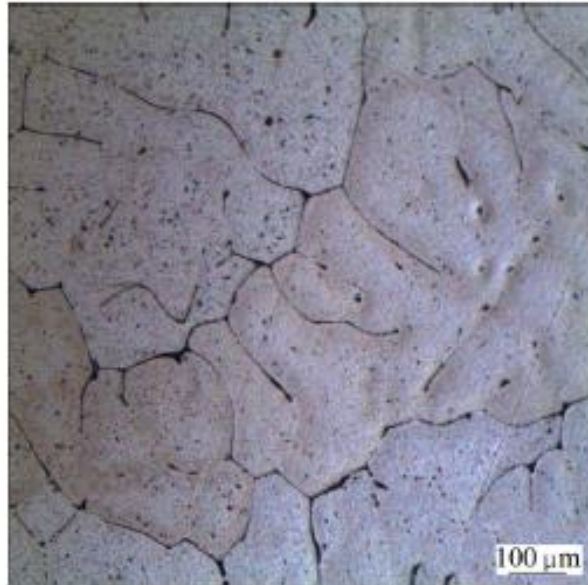


Figure 2.10: OM image of as-cast A11080 (Abd El Aal and Sadawy, 2015)

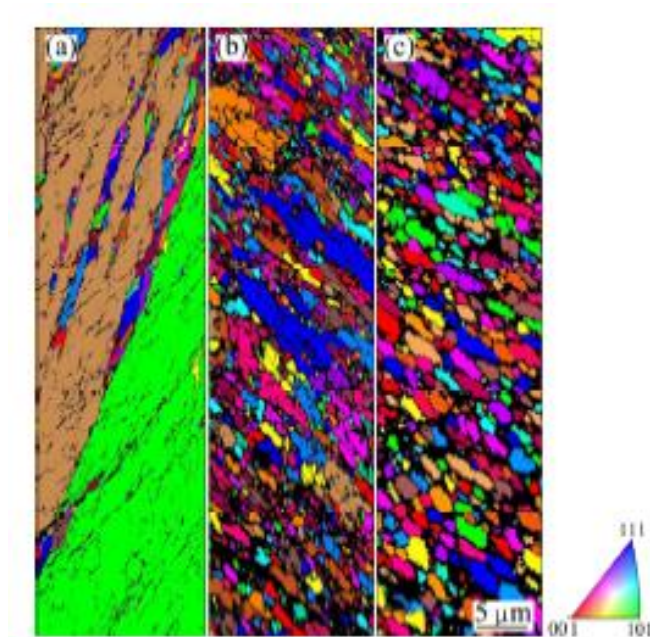


Figure 2.11: Color-coded orientation maps of deformed A11080 via ECAP at different number of passes, (a) 2 passes, (b) 4 passes and (c) 10 passes (Abd El Aal and Sadawy, 2015)

After ECAP process using route A, the microstructure of A11080 appeared to be elongated grains after 2 passes (Figure 2.11 (a)) and the average grain size reduced from 390 to 1.8 μm . It also consisted 27% of the grains are HAGB with 14° grain

boundaries misorientation angle as shown in Figure 2.12 (a). The microstructure of sample with 4 passes of ECAP process showed a combination of equiaxed and elongated grains. The average grain size of deformed A11080 up to 4 passes was to 0.4 μm and the fraction of HAGB increased from 27% to 50% with 25° value of the grain boundaries misorientation angle (Figure 2.12 (b)). Further grain refinement with 10 passes was observed and the grains are with 0.3 μm average grain size. Increased of the ECAP number appears to increase the average grain boundaries misorientation angle and the fraction of HAGB to 33° and 78% respectively. Hence, the increase number of ECAP passes is effective to produce UFG structure and equiaxed microstructure A110180 samples with HAGB (Abd El Aal and Sadawy, 2015).

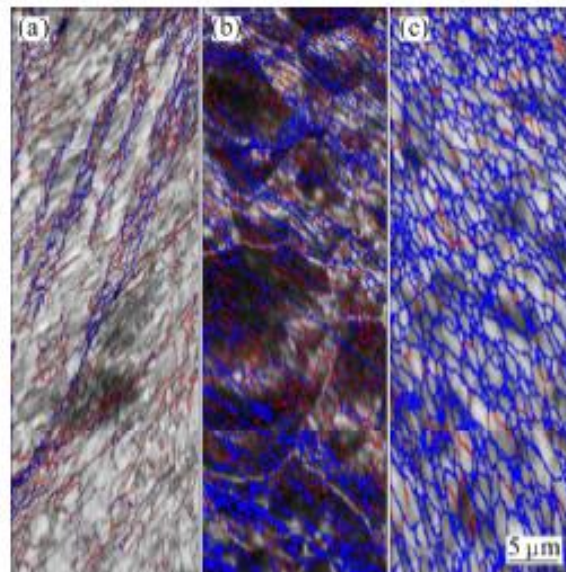


Figure 2.12: Color-coded grain boundaries maps of deformed A11080 via ECAP, (a) 2 passes, (b) 4 passes and (c) 10 passes (high angle $\geq 15^\circ$ with blue line and low angle $< 15^\circ$ with red line) (Abd El Aal and Sadawy, 2015)

2.7 Solderability

Solderability is the ability of the molten solder to wet on the surface and form beneficial joining in electronic applications. This means that a specific interaction will take place between the solid surface of the parts to be soldered and the liquid solder alloy (Abtey and Selvaduray, 2000). Solderability can be measured or assessed based on spreading area and wetting angle.

2.7.1 Spreading area or wetting angle

Spreading is defined as the ability of the molten solder to flow or spread over the part to be soldered during soldering process in order to have proper metallic bonding. The spreading process is also known as wetting of the liquid solder over a solid surface (Abtey and Selvaduray, 2000).

In wetting behavior, if the angle is between 0 to 90° the liquid is said to wet while 90 to 180° is considered as non-wetting. The wetting angle, θ provides measure of the quality of wetting and it can be represented using Young-Dupre equation:

$$\gamma_{vs} = \gamma_{sl} + \gamma_{lv} \cos \theta \quad \text{Equation 2.3}$$

where γ_{sv} is the surface tension of the solid and vapor, γ_{sl} is the surface tension of solid and liquid, and γ_{lv} is the surface tension of the liquid and vapour. Then, when $\theta < 90^\circ$ the liquid droplet will wet on the substrate and spread properly. The decrease of the wetting angle means an increase the spreading area (Humpston and Jacobson, 2004). Table 2.2 shows the criteria for evaluating the wetting angle for solder alloys. By referring to Satyanaran and Prabhu, (2013) found that wetting angle of SAC305 solder in the range $20^\circ \leq \theta \leq 30^\circ$ stated that it is very good to be used.

Table 2.2: Wetting categories of solder alloys (Mayhew and Wicks, 1971)

| Categories | Ranges |
|------------|--------------------------------------|
| Excellent | $0^\circ \leq \theta \leq 20^\circ$ |
| Very Good | $20^\circ \leq \theta \leq 30^\circ$ |
| Good | $30^\circ \leq \theta \leq 40^\circ$ |
| Adequate | $40^\circ \leq \theta \leq 55^\circ$ |
| Poor | $55^\circ \leq \theta \leq 70^\circ$ |
| Very Poor | $70^\circ \leq \theta \leq 90^\circ$ |

2.8 Mechanical testing

The mechanical properties of the solder materials used in electronic assemblies are important consideration to ensure the reliability of the solder joint. There are several methods used in order to evaluate the mechanical properties of solder interconnection. For example, microhardness test, tensile test, creep and lap joint test (Abteew and Selvaduray, 2000). These properties of solder alloys are dependent on the microstructure, intermetallic compounds and strain rate (Gu, et al., 2011).

2.8.1 Microhardness test

In hardness test, hardness is defined as the resistance to permanent deformation of the materials. In static indentation tests, the hardness can be measured by the relationship of load applied to a certain area or depth of indentation of the indenter such as in Brinell, Knoop, Rockwell and Vickers test (Chandler, 1999). The Vickers hardness test method use a diamond shape indenter and the indentation on materials is illustrated in Figure 2.13. The diamond indentation looks like a pyramid with square base and an angle of 136° and load applied on the materials is between 1 to 100 kgf. The load is applied for up to 10 to 15 seconds. The term of microhardness is referred to testing that uses indentation load not exceeding 1 kgf (Gordon, 1999).